A computational fluid dynamics analysis of the effects of size and shape of anterior nasal septal perforations*

Zainab Farzal[1], Anthony G. Del Signore[2], Adam M. Zanation[1], Charles S. Ebert, Jr. [1], Dennis Frank-Ito[3,4,5], Julia S. Kimbell[1], Brent A. Senior[1]

[1] Department of Otolaryngology/Head and Neck Surgery, University of North Carolina, Chapel Hill, NC, USA

[2] Department of Otolaryngology-Head and Neck Surgery, Mount Sinai Medical Center, New York, NY, USA

[3] Division of Head and Neck Surgery & Communication Sciences, Department of Surgery, Duke University Medical Center, Durham, NC, USA

[4] Computational Biology & Bioinformatics Program, Duke University, Durham, NC, USA

[5] Department of Mechanical Engineering and Materials Science, Duke University, Durham, NC, USA

Rhinology 57: 2, 153 -159, 2019

https://doi.org/10.4193/Rhin18.111

***Received for publication:**

May 24, 2018

Accepted: January 2, 2019

Abstract

Background: Nasal septal perforations (NSPs) often cause bleeding, crusting, obstruction, and/or whistling. The objective was to analyze the impact of anterior NSP size and shape on nasal physiology using computational fluid dynamics (CFD).

Methods: A 3-dimensional model of the nasal cavity was constructed from a radiologically normal CT scan using imaging software. Anterior NSPs (ovoid (ONSP): 0.5, 1, 2, and 3 cm long anterior-to-posteriorly and round (RNSP, 0.5 and 1 cm)) were virtually created in the model and divided into ventral, dorsal, anterior, and posterior regions. Steady-state inspiratory airflow, heat, and water vapor transport were simulated using Fluent™ CFD software. Air crossover through the perforation, wall shear, heat flux, water vapor flux, resistance, and humidification were analyzed.

Results: Air crossover and wall shear increased with perforation size. Regionally, wall shear and heat and water vapor flux were highest posteriorly and lowest anteriorly, generally increasing with size in those regions. RNSPs had greater heat and water vapor flux compared to corresponding size ONSPs. Resistance decreased by 10% or more from normal only in the 3 cm ONSP. Maximum water content was achieved more posteriorly in larger NSP nasal cavities.

Conclusions: High wall shear and heat and water vapor flux in posterior perforation regions may explain the crusting most commonly noted on posterior NSP edges. This preliminary study suggests that larger NSPs have a greater effect on nasal resistance and water content. Decrease in resistance with larger NSP size may be implicated in reported symptomatic improvement following enlargement of NSPs for treatment.

Key words: Computational Fluid Dynamics (CFD), nasal septum, nasal septal perforation, nasal airflow, wall shear, heat flux, humidification

Introduction

Nasal septal perforations (NSPs) result in a connection between nasal cavities creating an accessory pathway for airflow between the two nasal sides. NSPs are often iatrogenic occurring following nasal and sinus surgery or cauterization for epistaxis[(1)]. They also result from trauma, industrial exposure, nasal sprays, cocaine use, infections, or may be manifestations of systemic disease or malignancy[(1,2)]. The overall prevalence of NSPs is inadequately reported, but was found to be just under 1% in a large Scandinavian population[(3)] and as common as 35% in electroplating industry workers[(4)].

Physiologically, symptoms more frequently associated with NSPs include bleeding and crusting[(5)], which can cause significant discomfort often leading patients to manually remove dried blood or crusts and further exacerbating symptoms. NSP-associated airflow changes are believed to contribute to the sensation of

obstruction patients report[2]. Bleeding and crusting are more often noted when cartilage and mucoperichondrial layers are both exposed at perforation edges[5]. Since the perforation perimeter lies in the path of nasal airflow, understanding the interaction of airflow with perforation edges could lead to better treatments for perforation symptoms.

In recent years, the application of computational fluid dynamics (CFD) to the study of nasal airflow has enabled detailed examination of nasal physiology, providing new information on symptomatic alterations due to disease conditions or post-operative surgical changes. Three-dimensional (3D) anatomic models of the nasal cavity are created based on subject/patient-specific medical imaging which can then be used for computational modeling of aerodynamic patterns in the airway. Physiologic airflow and heat and water vapor transport can be simulated to provide an in-depth analysis of airflow distribution, nasal resistance, wall shear stress, heat and moisture exchange. CFD modeling has been validated for airflow measurements[6-13], and allow investigators to approximate perturbations of the nasal airway that can generate hypotheses and test sensitivities that would be difficult to discern by experimental measurement alone. Thus, despite not recapitulating living physiology explicitly, CFD models provide valuable information in the clinical setting.

Wall shear stress is a force exerted tangentially along a boundary by an adjacent moving fluid. In the nasal cavity, wall shear stress may be related to sensations of congestion, irritation, or pain via stimulation of mechanoreceptors[14], particularly in the septum. Heat and water vapor travel together in air and analysis of their flux at NSP edges yields key information about the heat/water exchange at the air-NSP interface. Heat and water vapor flux computation is distinct from that of humidification which represents the total content of water vapor in the air due to interactions with nasal cavity tissue including nasal walls, turbinates, and septum.

Several CFD studies have focused on the nasal alterations and symptoms observed with NSPs[15-23]. However, most of these studies analyzed changes either in single-sized perforations[15,16,19,20,22] or purely circular perforations[17,18,21], but anecdotally perforations are more commonly ovoid in shape. The objective of this study was to analyze the impact of size and shape (ovoid versus round) of anterior NSPs on nasal physiology using CFD simulations. In order to provide a comprehensive representation of physiologic changes due to anterior NSPs, we created four different sizes of ovoid and two different sizes of round anterior NSPs virtually in a normal nasal cavity. We compared airflow partitioning in each nasal side, air crossover through the perforation, nasal resistance, wall shear stress, humidification, and heat and water vapor transport in the models with and without NSPs.

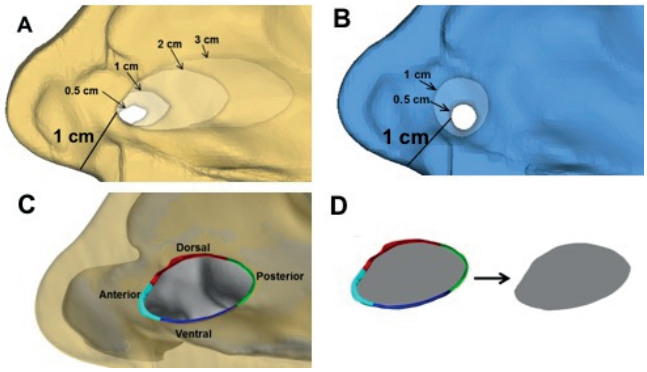

Figure 1. A. Visualization of the ONSP locations in a reconstruction in the plane of the septum. The anterior edge of each ONSP was located 1 cm from the columella. B. Location of RNSPs in the septum. The anterior edge of the 0.5 cm RNSP was located 1 cm from the columella. The anterior edge of the 1 cm RNSP was created 2 mm anterior to the 0.5 cm RNSP due to a septal ridge (8 mm from the columella). C. Regions of ONSP edges as shown in the 2 cm ONSP: anterior, posterior, dorsal, and ventral. External nares and septum are shown in semi-transparent sagittal view. Gray interior indicates nasal airspace. D. Sagittal cross section through the 2 cm ONSP illustrates planes used to visualize direction and speed of flow within the perforations.

Materials and methods

Three-dimensional reconstruction

A de-identified, radiologically normal CT scan of a 37-year-old female was imported into Mimics™ 17.0 imaging software (Materialise, Plymouth, MI). A 3D reconstruction of the nasal airway including the nostrils, nasal cavity, turbinates, and nasopharynx was made from which paranasal sinuses were excluded. Ovoid anterior NSPs of 0.5, 1, 2, and 3 cm length and 0.3, 0.6, 1.0, and 1.3 cm maximum height, respectively, were virtually created, with their long dimension on the anterior-to-posterior axis of the septum and their most anterior boundaries located 1 cm from the columella (Figure 1A). Two round NSPs, 0.5 and 1 cm in diameter, were similarly created; the anterior most boundary of the 0.5 cm perforation was 1 cm from the columella (Figure 1B). Due to a ridge in the septum, the 1 cm round perforation was created with its anterior border 8 mm from the columella. Larger size round NSPs were not feasible due to the limited height of the septum anteriorly. The ovoid shape was specifically chosen to mimic the shape of frequently seen NSPs and the anterior location was deemed most clinically relevant since most symptomatic NSPs occur anteriorly[24]. Additionally, round NSPs were included to study variation in physiology secondary to NSP shape. 3D reconstructions of the six NSP model airways and the original reconstruction were imported into the computer-aided design (CAD) and mesh generating software package ICEM-CFD™ 15.0 (ANSYS, Canonsburg, PA). The edge of each NSP was divided into four parts: anterior, posterior, ventral, and dorsal (Figure 1C, 1D).

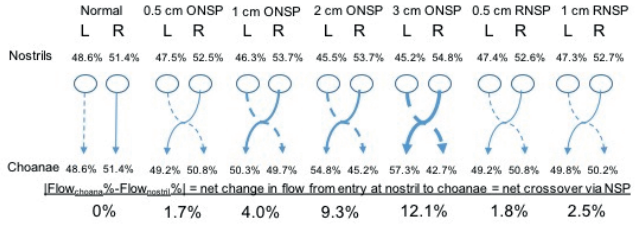

Figure 2. Net percent change in airflow on each side due to net air crossover from the right to the left via the NSPs.

Meshing and simulation

Planar surfaces at the nostrils and across the posterior nasopharynx were constructed for specifying inlet and outlet conditions on simulated airflow. Computational meshes of the airspaces, consisting of approximately 4 million unstructured, graded tetrahedral elements, were created. Steady-state, inspiratory airflow was simulated and analysis was performed using the CFD software package Fluent™ 15.0 (ANSYS, Inc., Canonsburg, PA, USA) under laminar conditions. Boundary conditions for airflow were as follows: a) the left and right nostrils were set as pressure inlets (gauge pressure of 0 Pa); b) the planar surface at the posterior nasopharynx was set as a pressure outlet with negative gauge pressure fitted to target a 15 Liters/minute flow rate; c) a no-slip condition (air velocity of zero) was set at nasal walls. Heat and water vapor transport, which are maximal during inspiratory flow, were simulated using the airflow simulation as input with inlet temperature of 293.15 K (20°C) and mass fraction of water at 0.00724 (50% relative humidity at 20°C). Outlet temperature was set to 305.75 K (32.6°C) and mass fraction of water to 0.03078 (100% relative humidity at 32.6°C). These boundary conditions have previously been validated in water and heat transport analysis by Garcia et al in 2007[25]. Airflow partitioning in each nasal side, nasal resistance, wall shear stress, humidification, and heat and water vapor flux were computed. Percent nasal humidification has been described previously[26], and was defined as:

$$\% \text{ humidification} = (C_{choanae} - C_{nostrils})/C_{mucosa} - C_{nostrils}) \times 100$$

where $C_{nostril}$, $C_{choanae}$, and C_{mucosa} are the water concentrations in air at the nostrils, choanae, and nasal mucosa surfaces, respectively. This quantity represents water transport from nasal mucosa during inspiration. Air crossover through the perforation was calculated as the difference between airflow at the level of the nostril and ipsilateral choana. Sagittal cross-sections through the perforations (Figure 1C) were made to visualize airflow direction and speed within the perforation using Fieldview™ 14.0 (Intelligent Light, Lyndhurst, PA, USA).

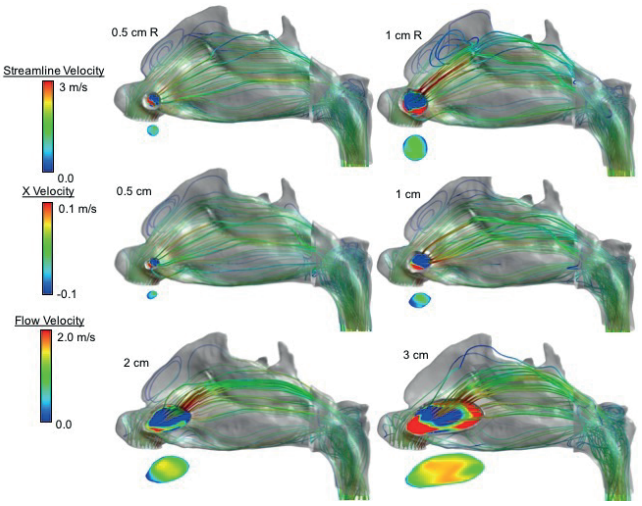

Figure 3. Sagittal view of each nasal airway showing airflow velocity streamlines with sagittal cross-sectional view of flow velocity. Cross-section within the airway model: magnitude of flow velocity in the plane of the NSP. Cross-section below airway model: airflow velocity component perpendicular to the plane of the NSP (X-direction; blue = -x, flow from subject's right to left toward viewer; red = +x, flow from subject's left to right away from viewer).

Results

In the original nasal airway model, a very slight right-sided predominance was noted with airflow partitioning: 51.4% and 48.6% on the right and left sides, respectively. This did not correspond to any discernable physical findings on CT such as nasal cycling, septal deviation, or mucosal/turbinate hypertrophy on the left. Air partitioning at the nostrils in the NSP models was consistently higher to the right side and increased with perforation size from 52.5% in 0.5 cm ONSP to 54.8% in the 3 cm ONSP (Figure 2). In RNSPs, small increases were noted in right side airflow partitioning of 52.6% in 0.5 cm RNSP to 52.7% in 1 cm RNSP.

Airflow crossover rate was described as the net percent increase in flow on the left side at the choana due to more air crossing left from the right than vice versa via the NSP. Airflow crossover increased with NSP size with the highest crossover rate of 12.1% for the 3 cm ONSP (Figure 2). The predominantly right-to-left airflow through the perforations was visually confirmed in each NSP (sagittal cross-section in each panel, Figure 3). The overall flow velocity magnitude was highest in the center-to-posterior regions of the 0.5 and 1 cm ONSPs and RNSPs and the middle of the 2 and 3 cm ONSPs (sagittal cross-section at bottom of each panel, Figure 3). Air also appeared to gain velocity just as it crossed the posterior border of the 1 cm RNSP and 1, 2, and 3 cm ONSPs (Figure 3).

Wall shear stress averaged over the entire edge of each NSP also increased with perforation size for both ONSPs and RNSPs. Regionally, wall shear was consistently highest along the

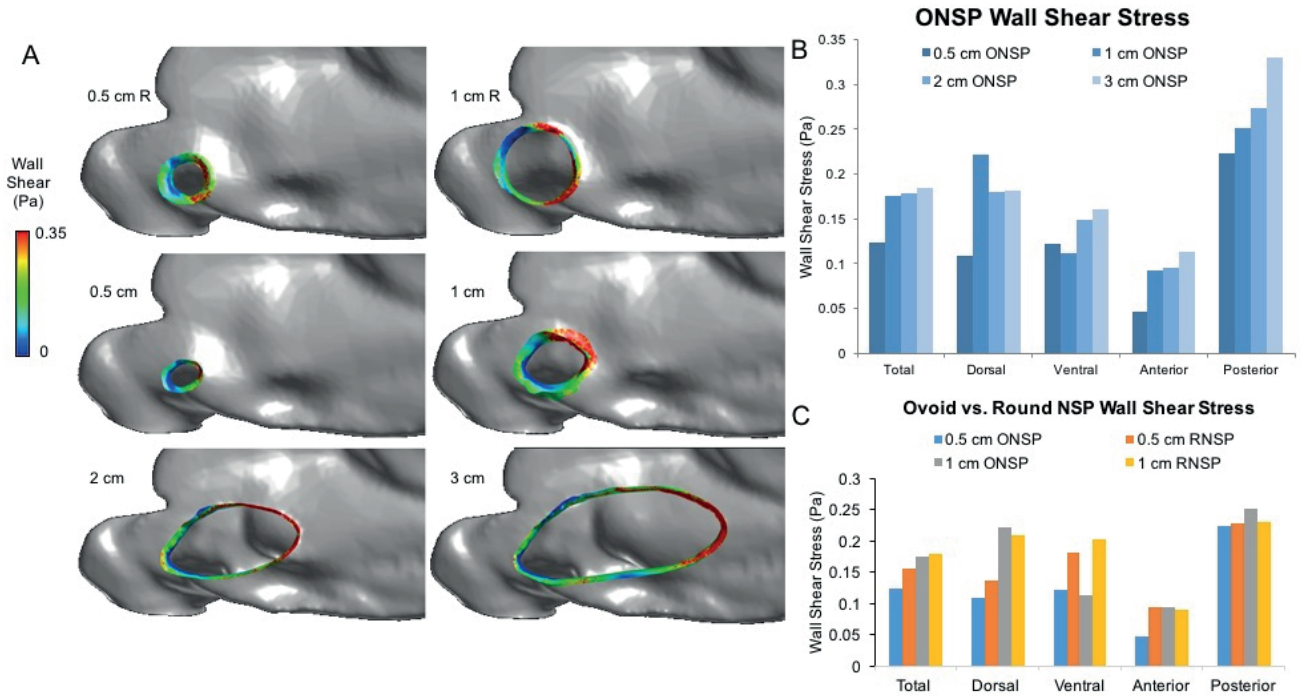

Figure 4. A. Mid-septal sagittal view of right side of nasal airspace (gray) showing wall shear stress distribution along each NSP edge. B. Total and regional wall shear stress at ONSP edges as a function of septal perforation size. C. Comparison of 0.5 and 1 cm ONSP and RNSP wall shear.

posterior edge of the perforation and lowest anteriorly, and increased with NSP size in those regions (Figure 4). Dorsal and ventral values did not correlate with size. When comparing percent increase in total wall shear stress at the perforation in the ONSPs, the greatest increase was noted between the 0.5 and 1 cm perforations (41.5%, Figure 4B). While overall and regional wall shear was higher in the 0.5 RNSP compared to the 0.5 ONSP, no consistent trend was noted when comparing the two 1 cm NSPs (Figure 4C).

Water and heat flux averaged over the right and left nasal sides varied only slightly with perforation size compared to normal. Averaged along the entire edge of each perforation, the highest heat and water vapor flux were noted in the 2 cm ONSP (Figure 5). Similar to wall shear stress, heat and water vapor flux were consistently highest posteriorly and lowest anteriorly, but there was no clear NSP size correlation (Figures 5 and 6). Both 0.5 and 1 cm RNSPs had greater total and regional heat and water vapor flux compared to their corresponding size ONSPs (Figure 5C, 5D). Total nasal cavity humidification had no evident correlation with perforation size and varied minimally from 93.1% to 96.9%. Likewise, average choanal temperature did not change appreciably with perforation size or shape (range: 305.13°K to 305.27°K). However, water content of air was measured along nasal cavity cross-sections for each ONSP and reached its maximum more posteriorly in the nasal cavity in larger ONSPs (2 and 3 cm) compared to smaller ONSPs (0.5 and 1 cm) (Figures 6 and 7).

Resistance decreased by 10% or more from normal only in the 3 cm ONSP case (11.1%) (Figure 8). The 1 cm ONSP airway had the highest resistance (0.043 Pa/(mL/s)) compared to the normal airway (0.040 Pa/(mL/s)) representing a 6.6% increase. Resistance for both RNSPs was unchanged from normal (0.040 Pa/(mL/s) each).

Discussion

Five similar CFD studies have previously analyzed nasal physiology in virtual, computational NSP models[15-18,21]. However, they have not specified size or exact location of NSP[15,21], reported on limited CFD physiologic parameters[16,17], or modeled only round NSPs[17,18]. Our current study differed by analyzing and comparing four ovoid and two round anterior, different-sized NSPs and their associated clinical implications to represent the most realistic, clinically probable scenarios. Virtual NSPs modeling allowed analysis of their effect on nasal cavity physiology without confounding effects from other findings such as septal deviation or turbinate hypertrophy that may coexist in scans of patients with true NSPs.

Air flow patterns have been a key feature of NSP physiology highlighted in the literature. As air velocity decreases along the anterior-posterior axis of the perforation, pooling of air further contributes to greater heat and water vapor flux posteriorly (discussed later). Furthermore, the sudden increase in velocity just as air crosses the posterior edge of the 1, 2, and 3 cm ONSPs may also correlate with bleeding and crusting. Three prior studies

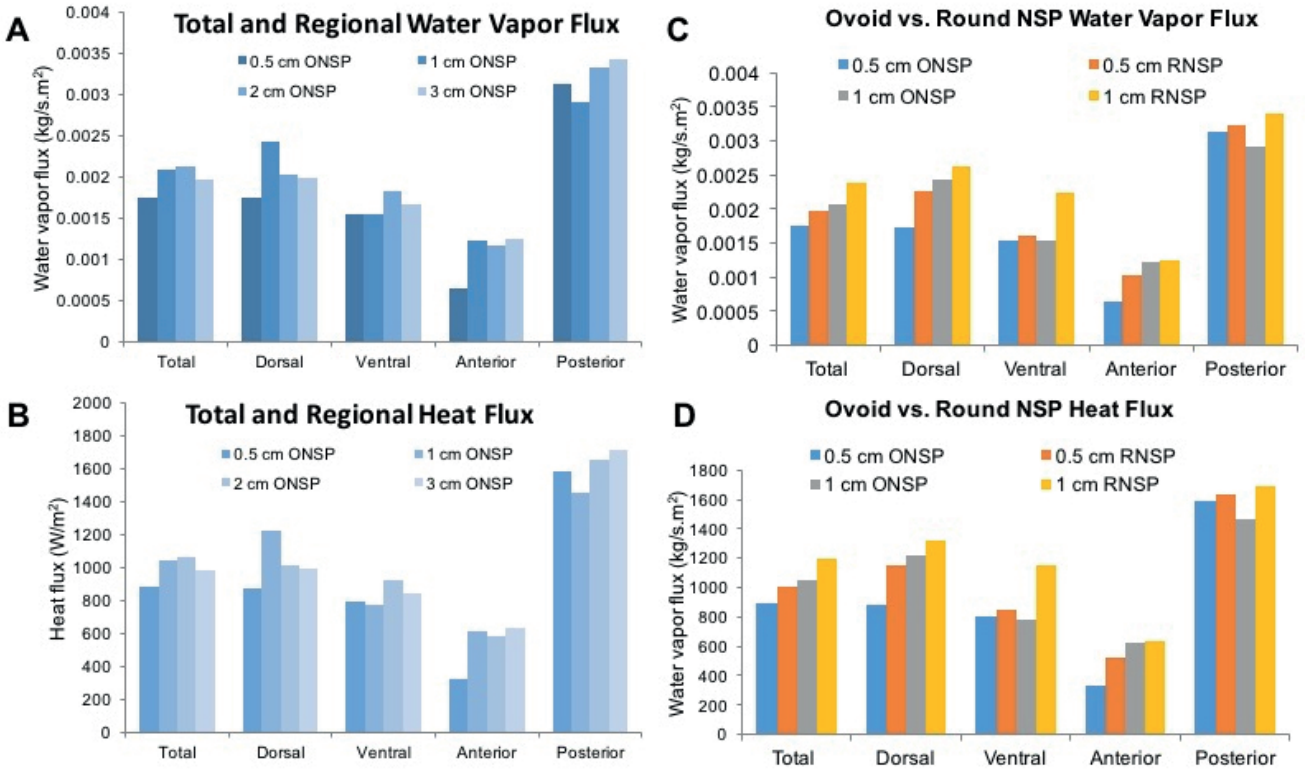

Figure 5. A. Total and regional water vapor flux at the edges of each ONSP as a function of NSP size. B. Total and regional heat flux at the edges of each ONSP as a function of NSP size. C. Comparison of 0.5 and 1 cm ONSP and RNSP water vapor flux. D. Comparison of 0.5 and 1 cm ONSP and RNSP heat flux.

have reported airflow crossover between nasal sides, but did not report extent of crossover or utilize a virtual model with equal or close to equal airflow partitioning[17,18,23]. Our study is the first to detail the extent of airflow crossover in virtual NSP models based on an airway with near equal flow allocation at baseline. We also noted that this crossover increased only 1% for a 55% increase in flow rate (2 cm case, data not shown). Resistance to airflow was noted to increase in the 1 cm NSP, but was lowest in the 3 cm NSP compared to the normal airway. Although resistance varied minimally amongst the NSPs (0.036-0.040 Pa/(mL/s)), the drop in resistance in the 3 cm NSP may provide the basis for reported symptom alleviation in patients who have had surgical enlargement of their NSPs which was demonstrated by Otto et al. in patients undergoing posterior septectomy[23,27].

Various wall shear stress findings have been reported, all of which correlated with bleeding[15,17,18]. Grant et al. suggested wall shear may also contribute to crusting[15]. We replicated the finding of Grant et al.[15] that highest wall shear occurred in the posterior edge of the NSP in all our NSP models. This pattern did not change with a 55% increase in inspiratory flow rate. Additionally, the observation that air crossing over through the NSP gains speed just as it crosses its posterior border likely contributes to wall shear and its symptomatic correlates of bleeding and crusting. A decrease in wall shear stress in the posterior region of NSPs after posterior septectomy or repair was shown by Otto et al. further supporting this theory[23]. High wall shear in the posterior NSP wall also corroborates previously reported higher levels of "disturbed airflow" in the middle and inferior turbinate regions[15]. Our study confirmed the finding of highest overall wall shear correlating with the largest anterior ONSP as first demonstrated by Cannon et al. in anterior RNSPs[18]. The present study was the first to highlight lowest wall shear anteriorly in each NSP with subsequent increase with increasing NSP size.

We sought to further elucidate the alterations in heat and water vapor flux which have not been characterized as extensively as wall shear stress. The correlation of high heat and water vapor flux posteriorly in all anterior NSPs likely contributes to the clinical observation of crusting usually occurring in the back of NSPs. High wall shear has been correlated with crusting previously[14], and our findings suggest that heat and water vapor flux may also play a role. Our study also presents another unique result: heat and water vapor flux averaged over the entire NSP did not correlate with perforation size. While only Otto et al.[23] have recently reported lack of correlation of heat flux with NSP size, this study is the first to report similar lack of correlation for water vapor flux. Additionally, this study is the first to clearly demon-

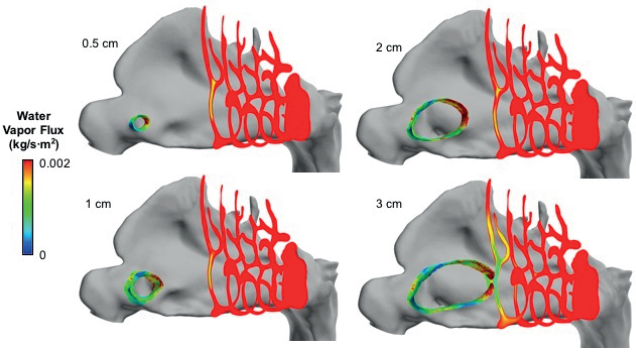

Figure 6. Water vapor flux modeled at ONSP edges and humidification in the posterior nasal cavity. Water vapor in air is demonstrated along nasal cavity cross-sections for each ONSP with the most anterior cross-section at the posterior edge of the 3 cm ONSP.

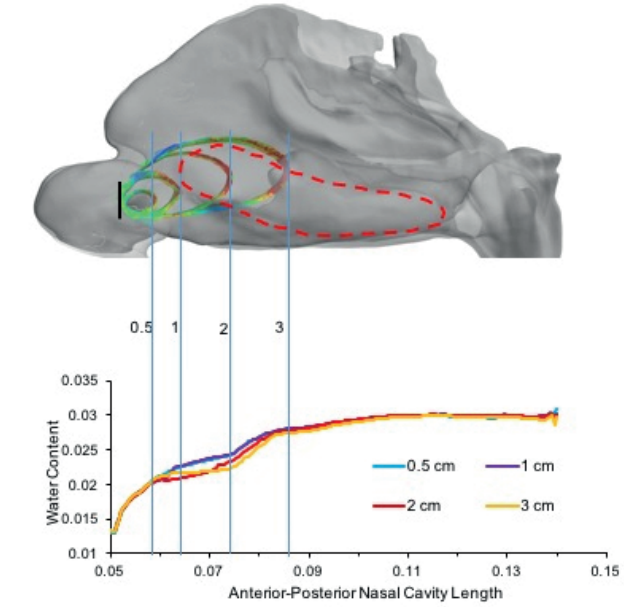

Figure 7. Water content along the nasal cavity in ONSPs. 3 cm ONSP nasal cavity model is scaled with its length corresponding to the x-axis of the graph below. Blue lines = posterior edge of each labeled ONSP. Black line demarks anterior most aspect of each ONSP. The dotted red line represents the outline of the inferior turbinate.

strate that water content in inhaled air reaches a maximum more posteriorly in subjects with larger ONSPs compared to those with smaller ONSPs, likely due to greater loss of surface area for water exchange. Importantly, this delay in humidification is demonstrated in the nasal cavity posterior to the 0.5 and 1 cm ONSPs and adjacent to the head of the inferior turbinate (Figure 8) emphasizing the more significant role of the internal nasal valve in humidification compared to the anterior nasal cavity. The highest heat and water vapor flux in the 2 cm ONSP may clinically correlate with the authors' anecdotal evidence that crusting most commonly occurs with mid-sized NSPs.

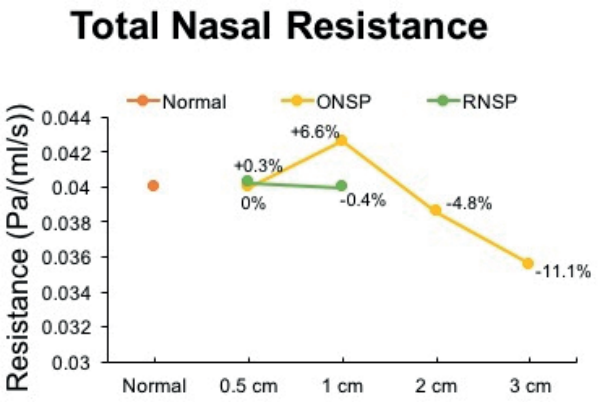

Figure 8. Resistance to airflow in NSP models between nares and choanae. Percentages provided represent percent change in resistance from the normal model.

Lastly, a comparison of ovoid and round, anterior NSPs is provided in this study. RNSPs consistently had greater heat and water vapor flux compared to their corresponding size ONSPs. Wall shear stress was also greater in the 0.5 cm RNSP, although the two 1 cm NSPs varied in magnitude by NSP regions. Notably, while the 1 cm ONSP had the greatest increase in resistance compared to the normal model, the 1 cm RNSP resistance was identical to the normal model resistance. Further studies are needed to characterize the reasons for these discrepancies.

This study has several limitations. First, it was based on a single individual's CT scan. As a result, the CFD findings can not be generalized to others due to inter-individual anatomic differences[13]. However, this highlights the previously demonstrated importance of providing subject sex and race data so that the applicability (external validity) of the findings can be assessed by the reader[28-30]. The findings presented here do agree with those of prior studies in different individuals[16-20]. Second, the models did not account for other adaptations that may occur in the nasal cavity such as mucosal and turbinate hypertrophy. However, as a result, we were able to demonstrate the isolated effects of perforations without confounding effects from such adaptations. Four recent studies have analyzed true NSPs and have compared physiologic parameters to post-virtual repair[19,20,22,23]. However, additional studies analyzing true NSPs are needed to provide a similar data library on physiologic alterations as we currently have for virtual NSPs.

Conclusion

The exploration of NSP physiology with CFD in the past decade has significantly enhanced our understanding of the nasal alterations that may cause patients' symptoms. High wall shear and heat and water vapor flux in posterior perforation regions may explain the occurrence of bleeding and crusting most com-

monly noted on posterior NSP edges. Further studies should correlate the complicated relationship of heat and water vapor flux with NSP size and shape. This preliminary study suggests that maximum humidification is achieved more posteriorly in the nasal cavity when larger NSPs are present. While modeling virtual NSPs has been useful, future CFD analysis of true NSPs using CT scans of individuals with perforations with comparison to demonstrated virtual NSP data will provide additional insight.

Acknowledgements

The authors thank Dr. Guilherme J. M. Garcia for his simulation protocol and user-defined functions to compute heat and water fluxes.

Authorship contribution

All authors contributed to the the conception/design of the work; the acquisition, analysis, and interpretation of data; drafting or revising the manuscript critically and approving the final version.

Conflict of interest

No conflicts of interest.

References

1. Kridel RW. Considerations in the etiology, treatment, and repair of septal perforations. Facial Plast Surg Clin North Am 2004; 12: 435-450.
2. Lanier B, Kai G, Marple B, Wall GM. Pathophysiology and progression of nasal septal perforation. Ann Allergy Asthma Immunol 2007; 99: 473-479.
3. Oberg D, Akerlund A, Johansson L, Bende M. Prevalence of nasal septal perforation: the Skovde population-based study. Rhinology 2003; 41: 72-75.
4. Lin SC, Tai CC, Chan CC, Wang JD. Nasal septum lesions caused by chromium exposure among chromium electroplating workers. Am J Ind Med 1994; 26: 221-228.
5. Kuriloff DB. Nasal septal perforations and nasal obstruction. Otolaryngol Clin North Am 1989; 22: 333-350.
6. Leong SC, Chen XB, Lee HP, Wang DY. A review of the implications of computational fluid dynamic studies on nasal airflow and physiology. Rhinology 2010; 48(2): 139-45.
7. Kim SK, Na Y, Kim JI, Chung SK. Patient specific CFD models of nasal airflow: overview of methods and challenges. J Biomech 2013; 46(2): 299-306.
8. Basu S, Frank-Ito DO, Kimbell JS. On computational fluid dynamics models for sinonasal drug transport: Relevance of nozzle subtraction and nasal vestibular dilation. Int J Numer Method Biomed Eng 2018; 34: e2946.
9. Kimbell JS, Segal RA, Asgharian B et al. Characterization of deposition from nasal spray devices using a computational fluid dynamics model of the human nasal passages. J Aerosol Med 2007; 20: 59-74.
10. Wofford MR, Kimbell JS, Frank-Ito DO et al. A computational study of functional endoscopic sinus surgery and maxillary sinus drug delivery. Rhinology 2015; 53: 41-48.
11. Craig JR, Zhao K, Doan N et al. Cadaveric validation study of computational fluid dynamics model of sinus irrigations before and after sinus surgery. Int Forum Allergy Rhinol 2016; 6: 423-428.
12. Li C, Jiang J, Dong H, Zhao K. Computational modeling and validation of human nasal airflow under various breathing conditions. J Biomech 2017; 64: 59-68.
13. Wen J, Inthavong K, Tu J, Wang S. Numerical simulations for detailed airflow dynamics in a human nasal cavity. Respir Physiol Neurobiol 2008; 161: 125-135.
14. Elad D, Naftali S, Rosenfeld M, Wolf M. Physical stresses at the air-wall interface of the human nasal cavity during breathing. J Appl Physiol (1985) 2006; 100: 1003-1010.
15. Grant O, Bailie N, Watterson J, et al. Numerical model of a nasal septal perforation. Stud Health Technol Inform 2004; 107: 1352-1356.
16. Pless D, Keck T, Wiesmiller KM, et al. Numerical simulation of airflow patterns and air temperature distribution during inspiration in a nose model with septal perforation. Am J Rhinol 2004; 18: 357-362.
17. Lee HP, Garlapati RR, Chong VF, Wang DY. Effects of septal perforation on nasal airflow: computer simulation study. J Laryngol Otol 2010; 124: 48-54.
18. Cannon DE, Frank DO, Kimbell JS, et al. Modeling nasal physiology changes due to septal perforations. Otolaryngol Head Neck Surg 2013; 148: 513-518.
19. Faramarzi M, Baradaranfar MH, Abouali O, et al. Numerical investigation of the flow field in realistic nasal septal perforation geometry. Allergy Rhinol (Providence) 2014; 5: 70-77.
20. Zhou B, Huang Q, Cui S, et al. Impact of airflow communication between nasal cavities on nasal ventilation. ORL J Otorhinolaryngol Relat Spec 2013; 75: 301-308.
21. Lindemann J, Rettinger G, Kroger R, Sommer F. Numerical simulation of airflow patterns in nose models with differently localized septal perforations. Laryngoscope 2013; 123: 2085-2089.
22. Nomura T, Ushio M, Kondo K, Yamasoba T. Effects of nasal septum perforation repair surgery on three-dimensional airflow: an evaluation using computational fluid dynamics. Eur Arch Otorhinolaryngol 2015; 272(11): 3327-33.
23. Otto BA, Li C, Farag AA, et al. Computational fluid dynamics evaluation of posterior septectomy as a viable treatment option for large septal perforations. Int Forum Allergy Rhinol 2017; 7: 718-725.
24. Diamantopoulos, II, Jones NS. The investigation of nasal septal perforations and ulcers. J Laryngol Otol 2001; 115: 541-544.
25. Garcia GJ, Bailie N, Martins DA, Kimbell JS. Atrophic rhinitis: a CFD study of air conditioning in the nasal cavity. J Appl Physiol (1985) 2007; 103(3): 1082-92.
26. Dayal A, Rhee JS, Garcia GJM. Impact of middle versus inferior total turbinectomy on nasal aerodynamics. Otolaryngol Head Neck Surg 2016; 155: 518-525.
27. Younger R, Blokmanis A. Nasal septal perforations. J Otolaryngol 1985; 14: 125-131.
28. Stephenson ED, Farzal Z, Zanation AM, Senior BA. Sex bias in rhinology research. Int Forum Allergy Rhinol 2018; 8(12): 1469-1475.
29. Stephenson ED, Farzal Z, Kilpatrick LA, Senior BA, Zanation AM. Sex bias in basic science and translational otolaryngology research Laryngoscope. 2018 Nov 8. doi: 10.1002/lary.27498.
30. Farzal Z, Stephenson ED, Senior BA, Zanation AM. Sex bias: Is it pervasive in otolaryngology clinical research? Laryngoscope. 2018 Nov 15. doi: 10.1002/lary.27497.

Zainab Farzal, MD
Department of Otolaryngology
Head & Neck Surgery
University of North Carolina at Chapel Hill
170 Manning Drive, CB #7070,
Physician's Office Building
Chapel Hill, NC, 27599
USA

Tel: +1-(919)966-6484
Fax: +1-(919)966-7941
E-mail:
Zainab.Farzal@unchealth.unc.edu